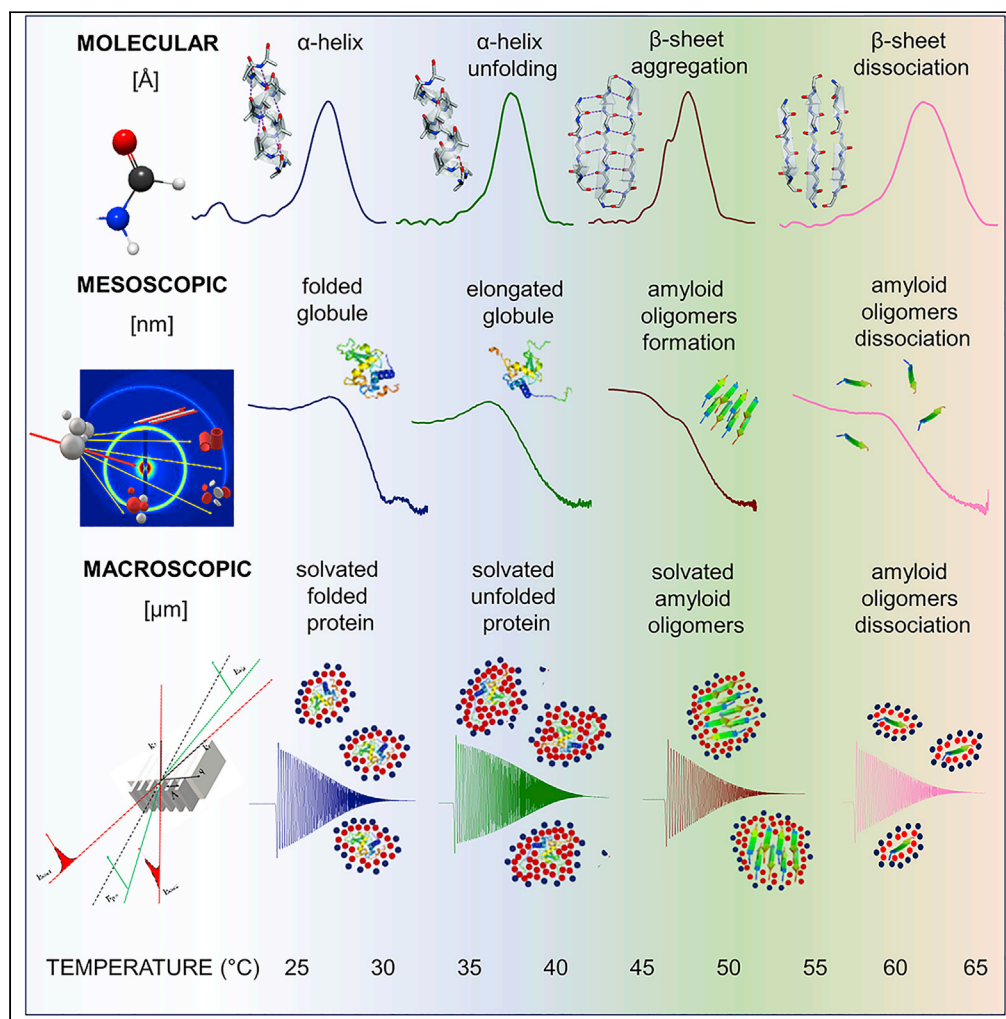**Article**

Multi-length scale structural investigation of lysozyme self-assembly

Sara Catalini,
Viviane Lutz-
Bueno, Mattia
Usuelli, ..., Marco
Paolantoni,
Raffaele
Mezzenga, Renato
Torre

catalini@lens.unifi.it (S.C.)
marco.paolantoni@unipg.it
(M.P.)
raffaele.mezzenga@hest.ethz.
ch (R.M.)
renato.torre@unifi.it (R.T.)

Highlights

Use of multi-length scale
spectroscopies to
characterize unstable
amyloid oligomers

Lysozyme form thermo-
labile amyloid oligomers
in self-crowded conditions

Amyloid oligomers
interact and form an
extended hydrogel
network

Amyloid oligomers are
responsible for the
existence of the hydrogel
matrix

iScience

Article

Multi-length scale structural investigation of lysozyme self-assembly

Sara Catalini,[1,2,9,*] Viviane Lutz-Bueno,[3,8] Mattia Usuelli,[3] Michael Diener,[3] Andrea Taschin,[2,4] Paolo Bartolini,[2,5] Paolo Foggi,[2,6] Marco Paolantoni,[6,*] Raffaele Mezzenga,[3,7,*] and Renato Torre[2,5,*]

SUMMARY

Reactive amyloid oligomers are responsible for cytotoxicity in amyloid pathologies and because of their unstable nature characterizing their behavior is a challenge. The physics governing the self-assembly of proteins in crowded conditions is extremely complex and its comprehension, despite its paramount relevance to understanding molecular mechanisms inside cells and optimizing pharmaceutical processes, remains inconclusive. Here, we focus on the amyloid oligomerization process in self-crowded lysozyme aqueous solutions in acidic conditions. We reveal that the amyloid oligomers form at high protein concentration and low pH. Through multi-length scale spectroscopic investigations, we find that amyloid oligomers can further interconnect with each other by weak and non-specific interactions forming an extended network that leads to the percolation of the whole system. Our multi-length scale structural analysis follows the thermal history of amyloid oligomers from different perspectives and highlights the impact of hierarchical self-assembly of biological macromolecules on functional properties.

INTRODUCTION

The transition of human soluble proteins into insoluble amyloid aggregates is the cause of an increasing number of degenerative amyloidogenic diseases (Chiti and Dobson, 2017). In parallel to this threating pathological frame, amyloid aggregates also perform functional roles in a wide span of living organisms, which range from bacteria to mammals (Knowles and Mezzenga, 2016). A deeper understanding of how nature synthesizes functional amyloids sheds light on the conditions in which pathological amyloids form. Additionally, amyloid structures can also be artificially synthetized *in vitro* and applied for designing novel functional materials with promising applications (Rajagopal and Schneider, 2004; Hanczyc et al., 2013; Mains et al., 2013; Bolisetty and Mezzenga, 2016; Chaves et al., 2016; Knowles and Mezzenga, 2016; Abdelrahman et al., 2020). Owing to the breadth of fields that seek an accurate definition of amyloid structures, pursuing fundamental and systematic studies on the proteins' hierarchical self-assembly mechanisms is of paramount importance.

A key factor is the specific molecular aggregation pathways that proteins experience during the hierarchical structuring from the molecular to the macroscopic length scales. At the molecular level, the structural building blocks that generate amyloid aggregates are independent of the protein type (Knowles and Mezzenga, 2016). They consist of amyloidogenic portions arranged into cross-β structures. At the mesoscopic length scale, amyloid aggregates reveal a wide morphological differentiation, like rigid fibers, curvilinear fibers, spheres, tubes, and so on, which depends on the pursued specific molecular aggregation pathway (Wei et al., 2017). The active research on amyloid aggregation points toward important aspects that should be further investigated. The first is the comprehension of the molecular paths that form reactive amyloid oligomers, indeed, because of their high cytotoxicity, the knowledge of the molecular steps leading to their formation could help design new inhibition strategies (Miti et al., 2015; Hasecke et al., 2018; Dear et al., 2020). The second concerns protein behavior in high concentrated environments, referred to here as crowded (>100 mg/mL) (Roosen-Runge et al., 2011; von Bülow et al., 2019). Crowded conditions are a requirement of several biotechnological topics, such as pharmaceutical formulation for the synthesis of monoclonal antibodies and understanding of proteins behavior in the cytoplasm of living cells with concentrations that can reach 400 mg/mL (Pastore and Temussi, 2012). At this level of crowding, the physical

mechanisms that govern protein behavior are highly complex, and physical parameters, such as excluded volume effect and molecular diffusion, become relevant to determine the hierarchical self-assembly pathways (Giugliarelli et al., 2016; McManus et al., 2016).

Here we address the complex processes occurring to proteins in self-crowded conditions through contactless and non-destructive spectroscopic techniques over multiple length scales. Previously, some of us used Fourier transform infrared (FTIR) spectroscopy to uncover the thermal denaturation and aggregation kinetics of highly concentrated solutions of the globular protein hen egg white lysozyme (LYS) (Catalini et al., 2021). Lysozyme has been chosen because is a small protein of 14.6 kDa often used as a model system to investigate the amyloid aggregation mechanisms owing to its propensity to form amyloid aggregates *in vitro*.

The present work unifies the molecular scale information from FTIR with the structural information in the nano and mesoscale obtained by small-angle X-ray scattering (SAXS). This approach enables us to describe the thermal unfolding, aggregation, and disaggregation processes of highly concentrated lysozyme solutions, and identify the molecular interactions that generate the oligomeric structures, together with their length scales. The balance between protein-protein and protein-solvent molecular interactions influences the size and the morphology of the formed nanoaggregates, and the macroscopic viscoelastic properties. The latter information is obtained by heterodyne transient grating (HD-TG) non-linear spectroscopy (Catalini et al., 2019). The multi-length scales probed through FTIR, SAXS and HD-TG provide an unprecedented overview of the hierarchical self-assembly of LYS solution in self-crowded condition and low pH. The complementary information provided by these spectroscopies enables deep insight into the unfolding of LYS structure, which is a necessary requirement for triggering all the other processes. The thermal history of the transient amyloid oligomers is revealed, and the possibility to generate an extended hydrogel network, in the thermodynamic region where the amyloid oligomers are stable, established. The weak and non-specific interactions among the amyloid oligomers are responsible for the hydrogel network and provide the thermal reversibility of the hydrogel phase.

RESULTS AND DISCUSSION
Thermal unfolding of self-crowded lysozyme solution

Unfolding relates to the exposition of the hydrophobic portions of protein monomers to the surrounding solvent. To examine the effect of crowding during the unfolding of LYS, we apply FTIR, SAXS, and time-resolved HD-TG on a self-crowded LYS solution, here referred to as LYS_{120} (120 mg of LYS in 1 mL of D_2O). Figures 1A–1C report the raw signals that cover the multi-length scales of the hierarchical system. We compare measurements at 25°C, when LYS monomers are in the folded state, to 70°C, when LYS monomers are in the unfolded state.

Focusing on the FTIR spectra (Figure 1A), we obtain molecular scale conformational changes in the LYS monomer owing to the unfolding process. The broad asymmetric peak centered at about 1650 cm^{-1} is the amide I (AmI) signal, which is mainly generated by the carbonyl stretching vibration. The carbonyl group of one amino acid residue, together with the aminic part of another residue, interacts and generates the so-called protein secondary structure. The carbonyl group interacts with the aminic portion to create secondary structural motifs such as α-helix, β-sheet, and turns (Pelton and McLean, 2000). Different secondary structures relate to different frequencies of carbonyl vibration, and lead to the consequent asymmetry of the amide I band. The percentage of unfolded LYS, obtained as described in the STAR Methods section (Sassi et al., 2011), is shown as a function of temperature (Figure 1D). The data identify the melting temperature of LYS at ∼51°C, when 50% of the protein structure is unfolded, in agreement with the previous analysis (Catalini et al., 2021).

Moving from the molecular to the mesoscopic length scale, information about the structural changes in the LYS globule is obtained through SAXS measurements (Figure 1B). In self-crowded conditions, the small-angle scattering intensity, I(q), is generated by two contributions: the form factor, P(q), and the structure factor, S(q). The first reflects intra-monomers electron density correlations and is used to extract information on the size and the shape of the monomers. The structure factor, S(q), reflects inter-monomers correlations and yields information about their interaction (Kikhney and Svergun, 2015). The concentrations at which the protein solutions were considered for the determination of the form factor ranged from 5 to 307 mg/mL (Figure S1). Both Figures 1B and S1 show a decrease in I(q) at small q-values for all the SAXS
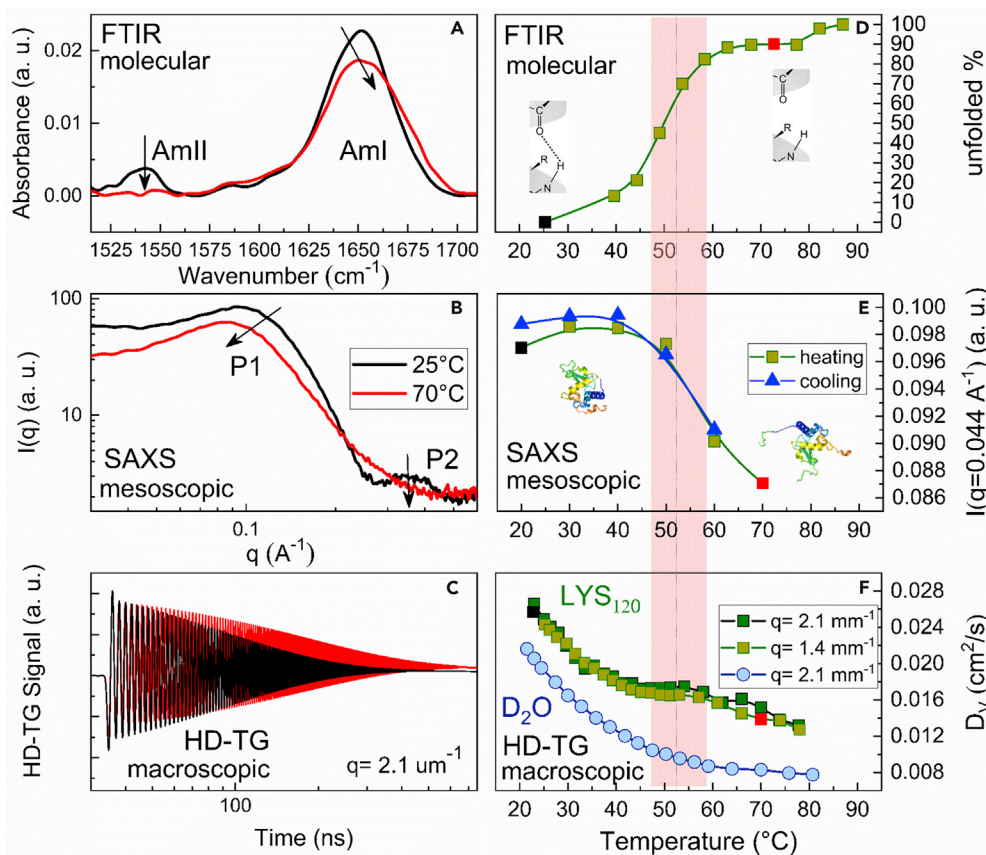
Figure 1. Thermal unfolding of self-crowded LYS solution

(A–C) Raw spectroscopic signals of the LYS_{120} solution at 25°C (black curves) and at 70°C (red curves), acquired using FTIR (A), SAXS (B), and HD-TG (C). Impact of temperature increase on the different parameters used to highlight the thermal behavior of the LYS_{120} solution.

(D) Percentage of unfolded LYS monomers as a function of temperature.

(E) Scattering vector (q) position of SAXS peak plotted vs temperature during heating (green points) and cooling (blue points) cycles.

(F) Viscosity coefficient, D_V, as a function of temperature at two different scattering vectors: 2.1 μm^{-1} and 1.4 μm^{-1}; the trend of D_V of the LYS_{120} solution is compared with the trend of the pure solvent, D_2O.

profiles, owing to inter-monomer repulsions. Only LYS with 5 mg/mL exhibits a plateau, characteristic of spherical form factor. These outputs highlight that for concentrations higher than 5 mg/mL, the monomers of LYS undergo a repulsive interaction potential (Bonnete et al., 1999; Finet et al., 2004). The SAXS curves have a broad peak between q = 0.1–0.2 Å^{-1} (identified as P1 in Figure 1B), related to the shape and size of the LYS monomer, and to the monomer-monomer correlation distance owing to the interactions among proteins (Kikhney and Svergun, 2015). With enhanced self-crowding (i.e., increasing concentration), the LYS monomers become closer, owing to the excluded volume effect, leading to lower correlation distances among them. This phenomenon is highlighted by the progressive shift at higher q value of broad peak (Figure S1), which reflects shorter correlation distances. Another broad peak, identified as P2 in Figure 1B, is present in the SAXS profiles between q = 0.3–0.6 Å^{-1}. This peak seems to be independent of the LYS concentration, and it reflects the structural inter-domain correlation related to the spatial disposition of the polypeptide chain, i.e. the protein tertiary structure (Hirai et al., 1998, 2004). We mainly relate P2 to the P(q) of folded monomers; however, we cannot exclude that it also has partial contributions from local peaks of S(q).

Figure 1E shows the q value at the maximum (q_{max}) of the P1 in the SAXS curves as a function of heating and cooling thermal cycles. This controls if LYS can recover its structure in such extreme conditions of low pH and self-crowding. The trend of q_{max} during heating points out that the SAXS signal at the length scale of

ca. 6 nm remains unchanged until 40°C, meaning that the LYS structure remains practically unaltered. At 50°C, the scattering curve moves toward lower q, as the globular protein unfolds and assumes in the unfolded state an extended spatial conformation. The thermal behavior of the SAXS curves in the self-crowded regime (Figure 1B) resembles the behavior found for the 5 mg/mL diluted LYS solution (Figure S2) and indicates that is mainly caused by variations of the form factor, dependent on the LYS globule elongation as a consequence of protein unfolding. Obviously, the temperature variation and the exposition of the protein hydrophobic portions influence the interaction potential and thus the structure factor, although to a lesser extent than the form factor. The persistence of P1 at the highest temperature of 90°C, Figure 1B, suggests that LYS monomers even if in an unfolded state retain certain globular compactness and are not fully denatured. Contrastingly, P2 disappears at high temperatures (Hirai et al., 1998; Arai and Hirai, 1999). We suggest that LYS elongation reduces specific intramolecular correlation distances between different domains. Moreover, the cooling curve follows the heating one, suggesting the high degree of structural reversibility of LYS even in the self-crowded regime (Figure S3).

As a control experiment, we compare these self-crowded results to the SAXS profiles obtained for the diluted LYS solutions using the same thermal ramp. We confirm the reversibility of the LYS structure (Figure S2). The molecular and structural changes of LYS in solution have a strong influence on the interactions occurring between the monomers and the surrounding hydration water molecules. Indeed, conformational changes have an impact on the macroscopic viscoelasticity, and therefore influence the propagation of the sound wave into the sample (Chiarelli et al., 2010, 2014). Figure 1C shows the HD-TG signal at low and high temperatures, whereas Figure 1F reports the thermal dependence of the viscosity coefficient, D_V, for the two investigated wave vectors, 2.1 μm^{-1} and 1.4 μm^{-1}, comparing the trend of the LYS$_{120}$ solution with that of the pure solvent. The viscosity coefficient is defined in the STAR Methods section and accounts for the viscoelasticity variation of the system. The temperature dependence of D_V shows a linear decrease until 45°C, like the thermal behavior of D_2O; however, while the D_2O signal continues to decrease between 50 and 60°C, the one of the protein solutions remains constant. The quasi-stationary value of D_V in the temperature range where the protein unfolding occurs is connected to the transition of the LYS monomers from the folded structural conformation to the unfolded one (Kessler and Dunn, 1969; Catalini et al., 2019). On one hand, enhanced thermal motion breaks the hydrogen bonds among water molecules more efficiently, leading to a viscosity drop. On the other hand, the temperature increase unfolds the protein globule with a consequent exposition of its hydrophobic parts. This process leads to a variation of the hydration shell, which increases the viscosity of the system (Kessler and Dunn, 1969; Pavlovskaya et al., 1992; Corredig and Dalgleish, 1996). These two competing effects determine the overall stationary value of D_V during the unfolding process.

To sum up, the processes involving proteins such as unfolding are highly dependent on thermodynamic variables and solvation environment. The protein concentration falls within these parameters. In our experimental conditions, the low solution pH strongly charges the surface of the LYS monomers (as LYS isoelectric point is at pH 11) and increases the repulsive potential among monomers, disfavouring the hierarchical self-assembly. We have verified that even at such high concentration (120 mg/mL) is possible to describe the unfolding process with a two-state model. At room temperature, LYS has a compact globular shape with the hydrophobic portions embedded into the core and has a positively charged surface. As the temperature increases, the chains acquire flexibility, but the overall structure remains practically unchanged up to 40°C. At 51°C, the greatest structural change occurs and the shape of the LYS monomers elongates becoming less globular. This structural variation causes the exposition of the hydrophobic portions to the solvent, generating an increase in the system viscosity. Even if the system is fully in a self-crowded regime, (> 100 mg/mL) there is no evidence of amyloid hierarchical self-assembly.

Thermal behavior of transient lysozyme amyloid oligomers

To increase the environmental crowding, we have studied a doubly concentrated LYS solution, here referred to as LYS$_{240}$ (240 mg of LYS in 1 mL of D_2O). Figure 2 combines the measurements performed with the three spectroscopic techniques on the sample LYS$_{240}$. Figures 2A–2C are acquired at temperatures of 25 and 60°C. Indeed, for temperatures higher than 60°C, two molecular pathways became relevant: one leads to the dissociation of the amyloid oligomer, and the other leads to amorphous self-assembly. The size of the amorphous aggregates, being presumably in the order of the wavelength of visible light, making the samples opaque and prevent the HD-TG signal recording, because of limitations in the used experimental geometry.
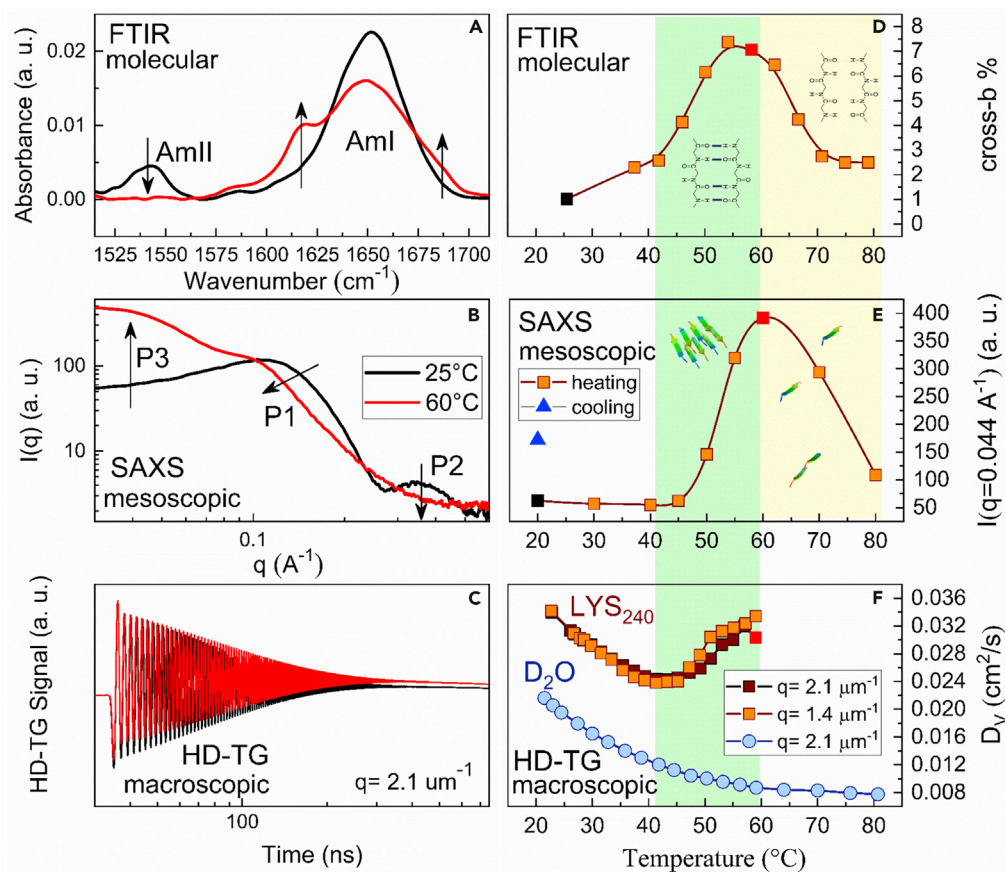
Figure 2. Thermal Behavior of Transient LYS Amyloid Oligomers

(A–C) Raw spectroscopic signals of the LYS_{240} solution at 25°C (black curves) and at 60°C (red curves), acquired using FTIR (A), SAXS (B), and HD-TG (C). Impact of temperature increase on the different parameters used to follow the hierarchical self-assembly process.

(D) Percentage of cross-β structures as a function of temperature.

(E) Scattering intensity value, I(q), at $q = 0.044\ A^{-1}$ plotted vs temperature during heating (orange points) and cooling (blue point).

(F) Viscosity coefficient, D_V, as a function of temperature at two different scattering vectors: 2.1 μm^{-1} and 1.4 μm^{-1}; the trend of D_V of LYS_{240} solution is compared with the trend of the pure solvent, D_2O.

The FTIR spectrum recorded at 60°C reported in Figure 2A clearly shows a peak at ca. 1620 cm^{-1}, which is a spectroscopic marker for intermolecular β-sheet interactions, considered a fingerprint of amyloids (Barth and Zscherp, 2002; Zandomeneghi et al., 2009; Sarroukh et al., 2013; Zou et al., 2013). Moreover, the presence of a shoulder at ca. 1690 cm^{-1} suggests antiparallel cross-β interactions (Barth and Zscherp, 2002; Zandomeneghi et al., 2009; Sarroukh et al., 2013; Zou et al., 2013). Self-crowded regime, low pH, and short waiting times of about 20 min favor the formation of small amyloid oligomers, both energetically and kinetically (Zou et al., 2013; Dear et al., 2020). Oligomers, after long waiting times of about 1 week, could evolve and form curvilinear fibrils (Mulaj et al., 2014; Miti et al., 2015; Cao et al., 2021). From the ratio of the areas of the intermolecular β-sheet signal and the whole amide I signal, a rough estimation of the percentage of intermolecular cross-β structures, with respect to the total amount of amide carbonyl groups is calculated (Figure 2D) as explained in more detail in the STAR Methods. The clearest evidence is that an unfolded protein structure is needed to stimulate the aggregation process. Once the cross-β aggregation starts, it rapidly evolves up to 55°C reaching the maximum number of amyloid oligomers. However, they are thermally unstable and dissociate at temperatures above 60°C. The possibility of dissociating amyloid aggregates at high temperature seems to be a quite peculiar feature of LYS (Sassi et al., 2011; Catalini et al., 2021), which is not common in all proteins (Cao et al., 2021; Comez et al., 2021). The formation of the amyloid oligomers has repercussion even at the mesoscopic length scale. Indeed, the SAXS recorded at 60°C

(Figure 2B) shows an enhancement of I(q) at low q-values owing to the hierarchical self-assembly of the LYS monomers that form amyloid oligomeric species. In fact, unfolded monomers self-assemble into these oligomers, which are larger than the individual building blocks, and scatter more at lower scattering vectors. Figure 2E reports the scattering intensity at a fixed wave vector, of $q = 0.044 A^{-1}$ as a function of temperature. It is the scattering vector at which the maximum increase in scattered intensity is found. The data plotted in Figures 2D and 2E show a similar trend as a function of temperature. This experimental evidence enables us to follow the thermal history of these transient species: oligomers with antiparallel cross-β structures develop at temperatures higher than 40°C and are most abundant between 50 and 55°C, with a size that falls within the length scales associated with the q-vectors with enhanced scattering signal, at about 14.2 nm ($2\pi/0.044 A^{-1}$). The comparison of the SAXS curves collected at 25°C before and after the thermal treatment is reported in Figure S5 and is superimposed in the middle-high scattering vector region, evidencing high structural reversibility of the protein monomer (Hirai et al., 1998; Arai and Hirai, 1999). A decrease of I(q) in the low q-region, for temperatures higher than 60°C, evidence that those amyloid oligomers are thermally stable until 60°C and for higher temperature dissociate, in agreement with the thermal trend observed for the cross-β signal in FTIR spectra (Figure 1D). These results suggest that LYS amyloid oligomers are small structures, mainly generated by thermo-labile cross-β interactions. The partial reversibility of the system is evidenced by the residual higher intensity at low q after cooling (Figure S5). Thus, while a large fraction of amyloid oligomers dissociates at higher temperatures, some aggregate remains after the thermal treatment.

The formation of amyloid oligomers has a strong influence on the viscoelastic properties of the whole system. The thermal behavior of the viscosity coefficient of the LYS$_{240}$ sample is shown in Figure 2F and is very different with respect to that of the LYS$_{120}$ solution where the hierarchical self-assembly does not occur. Above 40°C, the D$_V$ trend reverses and strongly increases with temperature, owing to the formation of amyloid oligomers (Corredig and Dalgleish, 1996; Corredig et al., 2004; Catalini et al., 2019). In fact, the formation of amyloid oligomers can contribute to damping the acoustic wave in the material: the most probable phenomenon is the overall increase of the viscosity of the solution, owing to the formation of weak physical interactions among the oligomers. Even the increase in the system complexity (Bryant and McClements, 1999a) and acoustic scattering phenomena could contribute (Bryant and McClements, 1999a, 1999b) to the acoustic wave damping.

To sum up, the increase of LYS concentration (double-concentration) allows the hierarchical self-assembly process. Even if the surface of protein is highly charged, self-crowding favors the interaction among LYS monomers. Concerning the molecular length-scale, FTIR data evidence the formation of antiparallel cross-β interactions among monomers, i.e. amyloid aggregates. The temporal scale of their growth (about 20 min and not 1 week) is compatible with the formation of small amyloid oligomers and not with long amyloid fibrils. Even the thermal instability of these aggregates is compatible with the formation of small labile oligomers. Information on the nanometre length scale confirms the molecular one and reveals that the oligomers' size is about 14.2 nm. Macroscopically, the growth of amyloid oligomers leads to an overall increase in the solution viscosity, which might be explained by considering their reciprocal interactions.

Thermal behavior of amyloid oligomer-based hydrogel

The formation of the amyloid oligomers and their propensity to interact with each other through weak interactions opens possibilities to design oligomeric-based hydrogels. The protocol for the hydrogel formation foresees leaving the LYS$_{240}$ solution at a high temperature (50°C) for 2 h, during which the amyloid oligomers are formed, and after a quick cooling of the sample, the system percolates forming a transparent hydrogel, hereafter referred to as GEL$_{50}$ (Catalini et al., 2021). This protocol enables the quick formation of the hydrogel, which has been exploited to investigate the thermal behavior of the amyloid oligomers that form the network gel matrix. The raw signals obtained through the three spectroscopic techniques are reported in Figures 3A–3C.

Figure 3D points out the evolution of the intermolecular β-sheet signal as a function of temperature, revealing the same thermal behavior found for the LYS$_{240}$ sample: the intermolecular β-sheet structures increase starting at ca. 45°C and then break at temperatures higher than 60°C. The SAXS profiles of the GEL$_{50}$ (Figure S6) sample match the outputs obtained through the FTIR spectra, revealing that both spectroscopic techniques can probe the transient amyloid oligomers directly in solution during their formation and dissociation (Figures 3D and 3F). The D$_V$ thermal trend, reported in Figure 3F, shows a marked change from 0.045
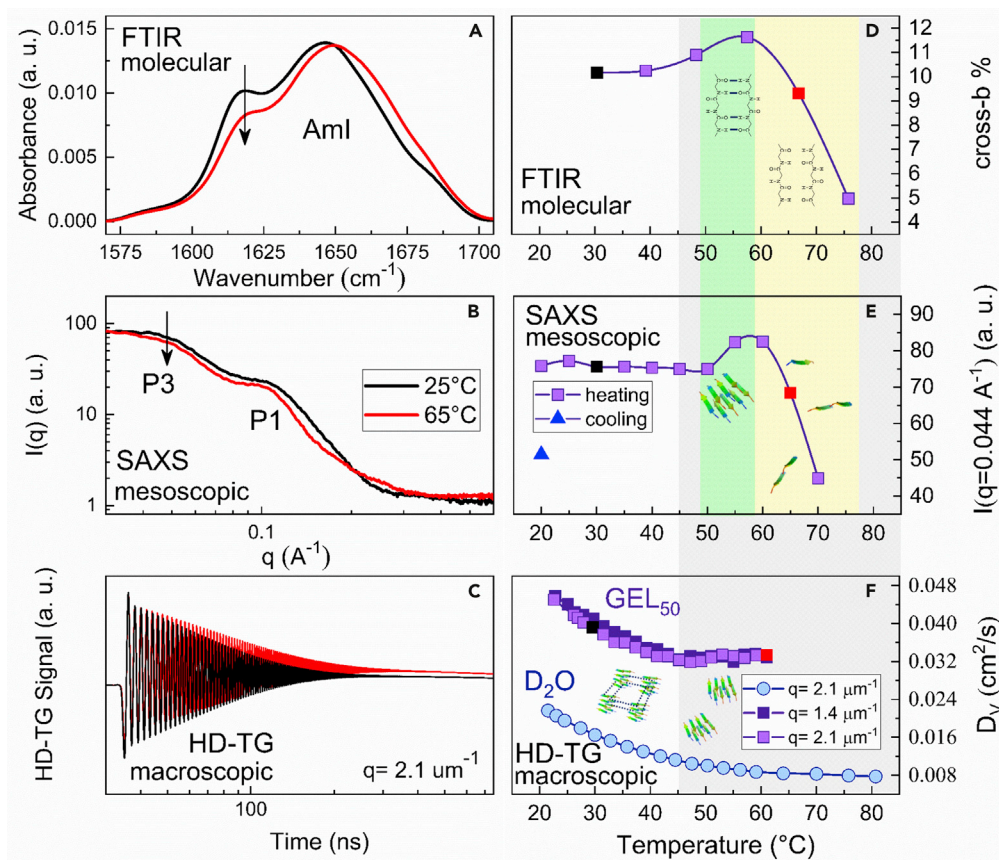
Figure 3. Thermal Behavior of Amyloid Oligomer-Based Hydrogel

(A–C) Raw spectroscopic signals of the GEL$_{50}$ sample at 25°C (black curves) and at 65°C (red curves), acquired using FTIR (A), SAXS (B), and HD-TG (C).

Impact of temperature increase on the different parameters used to follow the amyloid oligomers' thermal behavior.

(D) Percentage of cross-β structures as a function of temperature.

(E) Scattering intensity value, I(q), at q = 0.044 A^{-1} plotted vs temperature during heating (lilac points) and cooling (blue point).

(F) Viscosity coefficient, D$_V$, as a function of temperature at two different scattering vectors: 2.1 μm^{-1} and 1.4 μm^{-1}; the trend of D$_V$ of the GEL$_{50}$ sample is compared with the trend of the pure solvent, D$_2$O.

to 0.032 cm^2/s with temperature: D$_V$ decreases up to 45°C, and then a plateau appears at higher temperatures. The kink can be associated with the gel to liquid phase transition at 45°C (Catalini et al., 2021). In fact, the increase of the sound attenuation in the gel phase appears to be a generic occurrence of biologic systems, already observed in gelatine (Bacri et al., 1980; Dwyer et al., 2005; Parker and Povey, 2012) and in polysaccharides (Audebrand et al., 1995). Our data suggest the possibility to use HD-TG spectroscopy as non-destructive and contactless approach to follow phase transitions in biomaterials over length scales of 4-6 μm, as revealed by Figure S7 where the D$_V$ values of all the samples are plotted together.

The results obtained with the three different techniques can be rationalized, considering that there are two typologies of interactions that play a key role in the mentioned system. The first consists of cross-β motifs that self-assemble into oligomers, as probed by FTIR and SAXS experiments. The second consists of weak physical interactions such as hydrophobic and hydrogen bonds, which hold the oligomers together to form the gel matrix and is revealed by HD-TG. Up to 45°C, both interactions are present: cross-β motifs result from the quenching of LYS$_{240}$ solution at 50°C, and weak interactions provide elasticity to the hydrogel system. At 45°C, thermal energy breaks the weak interactions, driving consequently a gel-to-sol transition (Catalini et al., 2021), while cross-β motifs are further encouraged to form up to a temperature of 60°C. At higher temperatures, also the content of cross-β motifs decreases and the monomers assemble instead

into amorphous aggregates, the presence of which is suggested by the increased turbidity of the solution. Turbidity is related to the formation of structures with sizes in the order of the wavelength of light or larger.

Discussion on lysozyme clusters

To complete the discussion of our results it is important to analyze the relationship between our findings and previous observations about the presence or absence of clusters at low temperatures (between 5 and 25°C) in concentrated lysozyme suspensions (Sciortino et al., 2004; Cardinaux et al., 2007; Shukla et al., 2008). Both lysozyme and colloids were shown to form equilibrium clusters in concentrated states, owing to a subtle interplay between a short-ranged attraction potential and long-ranged electrostatic repulsion (Stradner et al., 2004). Experimental findings, based on X-ray and neutron scattering experiments, were corroborated through theoretical consideration and MD simulations (Sciortino et al., 2004; Cardinaux et al., 2007).

A later X-ray scattering work described the behavior of lysozyme in concentrated solutions through the introduction of a repulsive potential among individual monomers, however, without ascribing the features of the scattering functions to the presence of equilibrium clusters (Shukla et al., 2008).

In our experiments, the low pH of the solution (1.8) should prevent the formation of clusters. This consideration is based on the modeling of equilibrium clusters in lysozyme concentrated systems (Cardinaux et al., 2007), in which short-range attraction potential was modeled through a generalized Lennard-Jones potential (V_{SR}), while the long-range repulsion with a Yukava potential (V_Y). In the conditions of both the experimental works mentioned above (Stradner et al., 2004; Shukla et al., 2008) (pH = 7.8), the net charge of lysozyme molecules was assumed to be $Z_0 = +8e$. Such a pH condition leads to a repulsive potential that, at short distances (r/σ → 1), assumes a characteristic value $\frac{V_Y}{k_BT} \sim 2$, while the attraction potential has a minimum $\frac{V_{SR}}{k_BT} \sim -6$. The sum of the two potentials gives rise to a local minimum compatible with the inter-monomer distance in clusters.

At pH 1.8, the surface charge of lysozyme monomers was shown to double $Z_0 \sim +16e$ (Kuehner et al., 1999). As a consequence, as the Yukawa potential scales on Z_0 with a power of 2, the value of the potential increases of a factor 4 (neglecting the correction factor X, in Equation 2 in ref. (Cardinaux et al., 2007)). In these conditions, $\frac{V_Y}{k_BT} \sim 8$ and $\frac{V_{SR}}{k_BT} \sim -6$: the combination of the two potentials does not allow, therefore, a local minimum, which is compatible with the formation of equilibrium clusters.

Because of these latter considerations, the interpretation of the scattering data in the present work ascribed the peak in small-q regions ($q \sim 0.1$ A^{-1}) to the repulsive potential among monomers, while the peak in high-q regions ($q \sim 0.3 - 0.5$ A^{-1}) to intra-monomer features. In the latter case, the peak showed no dependency on concentration and disappeared on melting of the lysozyme monomers.

Conclusion

The multi-length scale spectroscopic approach here proposed, allows for a non-destructive and contactless *in situ* study of the processes involving proteins, and in general, biologic systems, proving to be an alternative and/or integrative method to the more conventional ones such as fluorescence, calorimetry, and rheology techniques. The coherent view, obtained by matching the outputs of the used spectroscopic techniques, allows for sketching the thermal history of the transient amyloid oligomers as pictured in Figure 4. The unfolding process follows the same molecular pathway regardless of the protein concentration, even if the macroscopic viscosity changes and unspecific transient clustering contacts could occur (Sciortino et al., 2004; Stradner et al., 2004; Liu et al., 2005; Shukla et al., 2008; Cardinaux et al., 2011; Assenza and Mezzenga, 2019). The thermal unfolding induces the exposition of the protein hydrophobic chains, which alter the arrangement of water molecules around the protein surface. For sufficient protein content, the exposure of the hydrophobic chains triggers the lysozyme aggregation in a controlled and specific way. The present experimental conditions (low pH and crowded conditions) favor the formation of transient amyloid oligomers with a relatively small size, which are composed by intermolecular β-sheet (Figure 4). The formed amyloid oligomers reveal a marked thermal instability and a tendency to interact among themselves by weak interactions. On the other hand, mature fibrils show high thermal stability and inertia (Chen et al., 2022). Our protocol for the preparation of the amyloid oligomer-based hydrogel is based on keeping the LYS$_{240}$ solution at 50°C for 2h to achieve a high content of amyloid oligomers and then
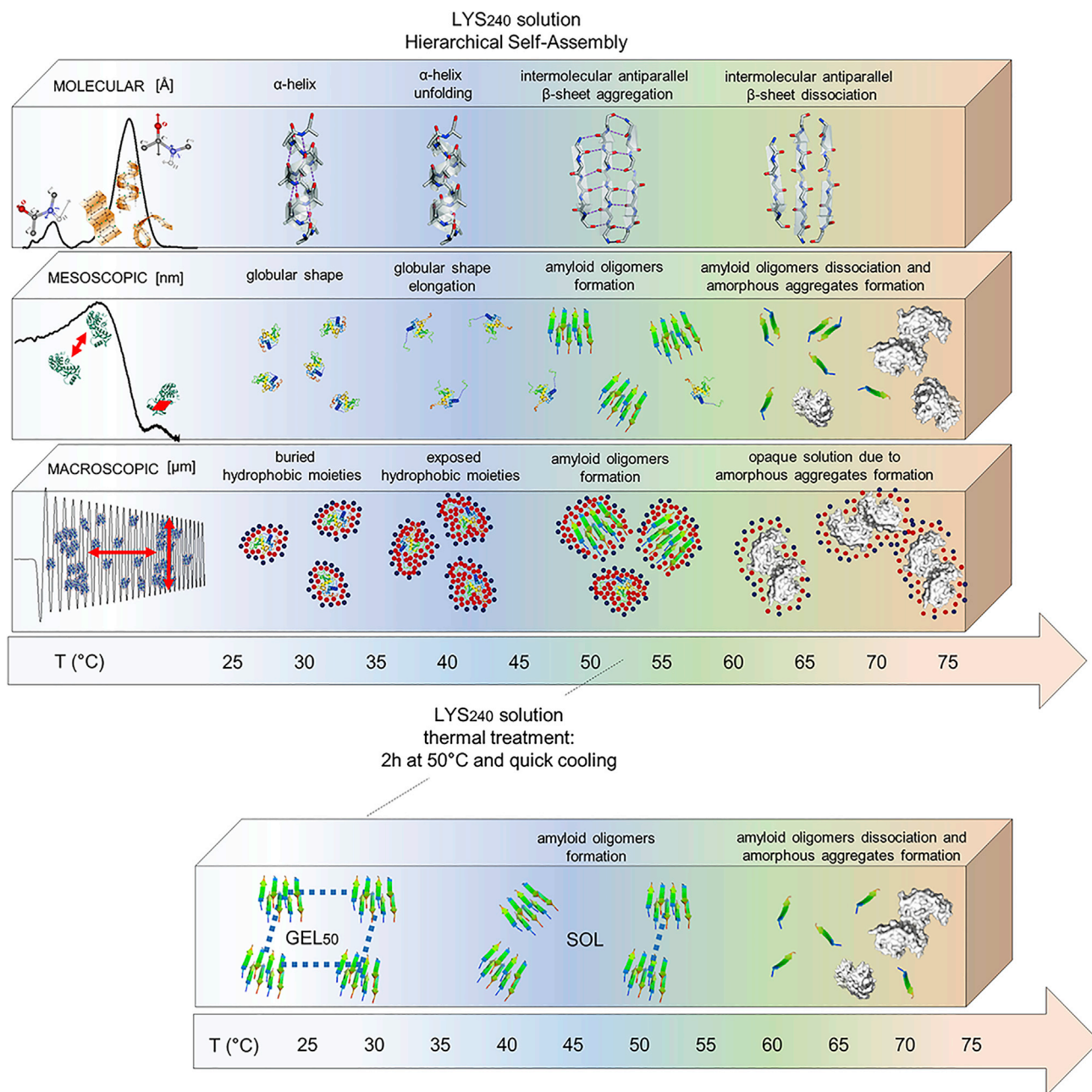
Figure 4. Thermal History of the Transient Amyloid Oligomers

Sketch of the thermal-induced hierarchical self-assembly of LYS$_{240}$ solution from the molecular (top side of the scheme) to the macroscopic length scale (bottom side of the scheme). The scheme of the protocol for the formation of the GEL$_{50}$ is reported in the bottom part of the figure. The incubation for 2h at 50°C of the LYS$_{240}$ solution guarantees the formation of high content of amyloid oligomers and the quick cooling at 25°C promotes the system percolation.

quickly cooling it at room temperature to incentivize the formation of the hydrogel network. The amyloid oligomers, which have been formed during the incubation of the solution at 50°C, can interact among them through weak bonds, forming an extended network that retains the water molecules and the non-aggregated lysozyme monomers inside the matrix, leading to the percolation of the system. Hydrogel based on amyloid oligomers transit to the liquid state at 45°C, as revealed by the D$_v$ thermal trend. Although the system starts to flow, the amyloid oligomers are still present and the intermolecular β-sheet

aggregation process restarts at 60°C (Catalini et al., 2021). The amyloid oligomers are responsible for the existence of the gel matrix, but they do not interact among them through cross-β interactions but rather through weak non-specific interactions that involve other portions of their structure.

Limitations of the study

Our *in situ* spectroscopic work investigates the self-assembly mechanism of lysozyme as a simple model protein. An important step forward could be to extend the proposed approach to other proteins in crowded conditions to infer the generality of the presented picture. Another improvement could be combining the spectroscopic techniques used in this work with a detailed morphological characterization of the hydrogel network.

STAR★METHODS

Detailed methods are provided in the online version of this paper and include the following:

- KEY RESOURCES TABLE
- RESOURCE AVAILABILITY
  - Lead contact
  - Materials availability
  - Data and code availability
- EXPERIMENTAL MODEL AND SUBJECT DETAILS
- METHOD DETAILS
  - Samples preparation
  - FTIR spectra
  - SAXS experiment
  - HD-TG experiment
- ADDITIONAL RESOURCES

SUPPLEMENTAL INFORMATION

Supplemental information can be found online at https://doi.org/10.1016/j.isci.2022.104586.

AUTHOR CONTRIBUTIONS

Conceptualization M.P.; Investigation S.C.; Resources M.P., P.F., R.M., and R.T.; Writing – Original Draft S.C.; Writing – Review & Editing S.C., V.L.B., M.U., M.D., A.T., P.B., P.F., M.P., R.M., and R.T.; Data Curation S.C., V.L.B., M.U., M.D., A.T., P.B., P.F., M.P., R.M., and R.T.; Visualization S.C.; Supervision M.P., R.M., and R.T.; Project Administration M.P., R.M., and R.T.; Funding Acquisition P.F. and R.T.

DECLARATION OF INTERESTS

The authors declare no competing interests.

INCLUSION AND DIVERSITY

We worked to ensure gender balance in the recruitment of human subjects. We worked to ensure sex balance in the selection of non-human subjects. While citing references scientifically relevant for this work, we also actively worked to promote gender balance in our reference list.

REFERENCES

Abdelrahman, S., Alghrably, M., Lachowicz, J.I., Emwas, A.H., Hauser, C.A.E., and Jaremko, M. (2020). "What doesn't kill you makes you stronger": future applications of amyloid aggregates in biomedicine. Molecules 25, 5245. https://doi.org/10.3390/molecules25225245.

Arai, S., and Hirai, M. (1999). Reversibility and hierarchy of thermal transition of hen egg-white lysozyme studied by small-angle X-ray scattering. Biophys. J. 76, 2192–2197. https://doi.org/10.1016/S0006-3495(99)77374-1.

Assenza, S., and Mezzenga, R. (2019). Soft condensed matter physics of foods and macronutrients. Nat. Rev. Phys. 1, 551–566. https://doi.org/10.1038/s42254-019-0077-8.

Audebrand, M., Doublier, J.L., Durand, D., and Emery, J.R. (1995). Investigation of gelation phenomena of some polysaccharides by ultrasonic spectroscopy. Food Hydrocoll. 9, 195–203. https://doi.org/10.1016/S0268-005X(09)80216-6.

Bacri, J.C., Courdille, J.M., Dumas, J., and Rajaonarison, R. (1980). Ultrasonic waves: a tool for gelation process measurements. J. Phys. Lett. 41, 369–372. https://doi.org/10.1051/jphyslet:019800041015036900.

Barth, A., and Zscherp, C. (2002). What vibrations tell about proteins. Q. Rev. Biophys. 35, 369–430. https://doi.org/10.1017/S0033583502003815.

Bolisetty, S., and Mezzenga, R. (2016). Amyloid–carbon hybrid membranes for universal water purification. Nat. Nanotechnol. 11, 365–371. https://doi.org/10.1038/nnano.2015.310.

Bonneté, F., Finet, S., and Tardieu, A. (1999). Second virial coefficient: variations with lysozyme crystallization conditions. J. Cryst. Growth 196, 403–414. https://doi.org/10.1016/S0022-0248(98)00826-4.

Bryant, C.M., and McClements, D.J. (1999a). Ultrasonic spectrometry study of the influence of temperature on whey protein aggregation. Food Hydrocoll. 13, 439–444. https://doi.org/10.1016/S0268-005X(99)00018-1.

Bryant, C.M., and McClements, D.J. (1999b). Ultrasonic spectroscopy study of relaxation and scattering in whey protein solutions. J. Sci. Food Agric. 79, 1754–1760. https://doi.org/10.1002/(SICI)1097-0010(199909)79:12<1754::AID-JSFA438>3.0.CO;2-D.

von Bülow, S., Siggel, M., Linke, M., and Hummer, G. (2019). Dynamic cluster formation determines viscosity and diffusion in dense protein solutions. Proc. Natl. Acad. Sci. U S A 116, 9843–9852. https://doi.org/10.1073/pnas.1817564116.

Cao, Y., Adamcik, J., Diener, M., Kumita, J.R., and Mezzenga, R. (2021). Different folding states from the same protein sequence determine reversible vs irreversible amyloid fate. J. Am. Chem. Soc. 143, 11473–11481. https://doi.org/10.1021/jacs.1c03392.

Cardinaux, F., Stradner, A., Schurtenberger, P., Sciortino, F., Zaccarelli, E., and StrAdner, A. (2007). Modeling equilibrium clusters in lysozyme solutions. Europhys. Lett. 77, 48004. https://doi.org/10.1209/0295-5075/77/48004.

Cardinaux, F., Zaccarelli, E., Stradner, A., Bucciarelli, S., Farago, B., Egelhaaf, S.U., Sciortino, F., and Schurtenberger, P. (2011). Cluster-driven dynamical arrest in concentrated lysozyme solutions. J. Phys. Chem. B 115, 7227–7237. https://doi.org/10.1021/jp112180p.

Catalini, S., Taschin, A., Bartolini, P., Foggi, P., and Torre, R. (2019). Probing globular protein self-assembling dynamics by heterodyne transient grating experiments. Appl. Sci. 9, 405. https://doi.org/10.3390/app9030405.

Catalini, S., Perinelli, D.R., Sassi, P., Comez, L., Palmieri, G.F., Morresi, A., Bonacucina, G., Foggi, P., Pucciarelli, S., and Paolantoni, M. (2021). Amyloid self-assembly of lysozyme in self-crowded conditions: the Formation of a protein oligomer hydrogel. Biomacromolecules 22, 1147–1158. https://doi.org/10.1021/acs.biomac.0c01652.

Chaves, S., Pera, L.M., Avila, C.L., Romero, C.M., Baigori, M., Morán Vieyra, F.E., Borsarelli, C.D., and Chehin, R.N. (2016). Towards efficient biocatalysts: photo-immobilization of a lipase on novel lysozyme amyloid-like nanofibrils. RSC Adv. 6, 8528–8538. https://doi.org/10.1039/c5ra19590j.

Chen, Y., Liu, Q., Yang, F., Yu, H., Xie, Y., and Yao, W. (2022). Lysozyme amyloid fibril: regulation, application, hazard analysis, and future perspectives. Int. J. Biol. Macromol. 200, 151–161. https://doi.org/10.1016/j.ijbiomac.2021.12.163.

Chiarelli, P., Lanatà, A., Carbone, M., and Domenici, C. (2010). High frequency poroelastic waves in hydrogels. J. Acoust. Soc. Am. 127, 1197–1207. https://doi.org/10.1121/1.3293000.

Chiarelli, P., Vinci, B., Lanatà, A., Lagomarsini, C., and Chiarelli, S. (2014). Poroelastic longitudinal wave equation for soft living tissues. J. Biorheol. 28, 29–37. https://doi.org/10.17106/jbr.28.29.

Chiti, F., and Dobson, C.M. (2017). Protein misfolding, amyloid formation, and human disease: a summary of progress over the last decade. Annu. Rev. Biochem. 86, 27–68. https://doi.org/10.1146/annurev-biochem-061516-045115.

Comez, L., Gentili, P.L., Paolantoni, M., Paciaroni, A., and Sassi, P. (2021). Heat-induced self-assembling of BSA at the isoelectric point. Int. J. Biol. Macromol. 177, 40–47. https://doi.org/10.1016/j.ijbiomac.2021.02.112.

Corredig, M., Alexander, M., and Dalgleish, D.G. (2004). The application of ultrasonic spectroscopy to the study of the gelation of milk components. Food Res. Int. 37, 557–565. https://doi.org/10.1016/j.foodres.2003.12.011.

Corredig, M., and Dalgleish, D.G. (1996). Effect of temperature and pH on the interactions of whey proteins with casein micelles in skim milk. Food Res. Int. 29, 49–55. https://doi.org/10.1016/0963-9969(95)00058-5.

Dear, A.J., Michaels, T.C.T., Meisl, G., Klenerman, D., Wu, S., Perrett, S., Linse, S., Dobson, C.M., and Knowles, T.P.J. (2020). Kinetic diversity of amyloid oligomers. Proc. Natl. Acad. Sci. U S A 117, 12087–12094. https://doi.org/10.1073/pnas.1922267117.

Dwyer, C., Donnelly, L., and Buckin, V. (2005). Ultrasonic analysis of rennet-induced pre-gelation and gelation processes in milk. J. Dairy Res. 72, 303–310. https://doi.org/10.1017/S0022029905001020.

Finet, S., Skouri-Panet, F., Casselyn, M., Bonneté, F., and Tardieu, A. (2004). The Hofmeister effect as seen by SAXS in protein solutions. Curr. Opin. Colloid Interface Sci. 9, 112–116. https://doi.org/10.1016/j.cocis.2004.05.014.

Giugliarelli, A., Urbanelli, L., Ricci, M., Paolantoni, M., Emiliani, C., Saccardi, R., Mazzanti, B., Lombardini, L., Morresi, A., and Sassi, P. (2016). Evidence of DMSO-induced protein aggregation in cells. J. Phys. Chem. A 120, 5065–5070. https://doi.org/10.1021/acs.jpca.6b00178.

Hanczyc, P., Samoc, M., and Norden, B. (2013). Multiphoton absorption in amyloid protein fibres. Nat. Photon. 7, 969–972. https://doi.org/10.1038/nphoton.2013.282.

Hasecke, F., Miti, T., Perez, C., Barton, J., Schölzel, D., Gremer, L., Grüning, C.S.R., Matthews, G., Meisl, G., Knowles, T.P.J., et al. (2018). Origin of metastable oligomers and their effects on amyloid fibril self-assembly. Chem. Sci. 9, 5937–5948. https://doi.org/10.1039/c8sc01479e.

Hirai, M., Arai, S., Iwase, H., and Takizawa, T. (1998). Small-angle X-ray scattering and calorimetric studies of thermal conformational change of lysozyme depending on pH. J. Phys. Chem. B 102, 1308–1313. https://doi.org/10.1021/jp9713367.

Hirai, M., Koizumi, M., Hayakawa, T., Takahashi, H., Abe, S., Hirai, H., Miura, K., and Inoue, K. (2004). Hierarchical map of protein unfolding and refolding at thermal equilibrium revealed by wide-angle X-ray scattering. Biochemistry 43, 9036–9049. https://doi.org/10.1021/bi0499664.

Kessler, L.W., and Dunn, F. (1969). Ultrasonic investigation of the conformal changes of bovine serum albumin in aqueous solution. J. Phys. Chem. 73, 4256–4263. https://doi.org/10.1021/j100846a037.

Kikhney, A.G., and Svergun, D.I. (2015). A practical guide to small angle X-ray scattering (SAXS) of flexible and intrinsically disordered proteins. FEBS Lett. 589, 2570–2577. https://doi.org/10.1016/j.febslet.2015.08.027.

Knowles, T.P.J., and Mezzenga, R. (2016). Amyloid fibrils as building blocks for natural and artificial functional materials. Adv. Mater. 28, 6546–6561. https://doi.org/10.1002/adma.201505961.

Kuehner, D.E., Engmann, J., Fergg, F., Wernick, M., Blanch, H.W., and Prausnitz, J.M. (1999). Lysozyme net charge and ion binding in concentrated aqueous electrolyte solutions. J. Phys. Chem. B 103, 1368–1374. https://doi.org/10.1021/jp983852i.

Liu, Y., Fratini, E., Baglioni, P., Chen, W.R., and Chen, S.H. (2005). Effective long-range attraction between protein molecules in solutions studied by small angle neutron scattering. Phys. Rev. Lett. 95, 118102. https://doi.org/10.1103/PhysRevLett.95.118102.

Mains, J., Lamprou, D.A., McIntosh, L., Oswald, I.D.H., and Urquhart, A.J. (2013). Beta-adrenoceptor antagonists affect amyloid nanostructure; amyloid hydrogels as drug delivery vehicles. Chem. Commun. 49, 5082. https://doi.org/10.1039/c3cc41583j.

McManus, J.J., Charbonneau, P., Zaccarelli, E., and Asherie, N. (2016). The physics of protein self-assembly. Curr. Opin. Colloid Interface Sci. 22, 73–79. https://doi.org/10.1016/j.cocis.2016.02.011.

Miti, T., Mulaj, M., Schmit, J.D., and Muschol, M. (2015). Stable, metastable, and kinetically trapped amyloid aggregate phases. Biomacromolecules 16, 326–335. https://doi.org/10.1021/bm501521r.

Mulaj, M., Foley, J., and Muschol, M. (2014). Amyloid oligomers and protofibrils, but not filaments, self-replicate from native lysozyme. J. Am. Chem. Soc. 136, 8947–8956. https://doi.org/10.1021/ja502529m.

Parker, N.G., and Povey, M.J.W. (2012). Ultrasonic study of the gelation of gelatin: phase diagram, hysteresis and kinetics. Food Hydrocoll. 26, 99–107. https://doi.org/10.1016/j.foodhyd.2011.04.016.

Pastore, A., and Temussi, P.A. (2012). The two faces of Janus: functional interactions and protein aggregation. Curr. Opin. Struct. Biol. 22, 30–37. https://doi.org/10.1016/j.sbi.2011.11.007.

Pavlovskaya, G., McClements, D.J., and Povey, M.J.W. (1992). Ultrasonic investigation of aqueous solutions of a globular protein. Food Hydrocoll. 6, 253–262. https://doi.org/10.1016/S0268-005X(09)80093-3.

Pelton, J.T., and McLean, L.R. (2000). Spectroscopic methods for analysis of protein secondary structure. Anal. Biochem. 277, 167–176. https://doi.org/10.1006/abio.1999.4320.

Rajagopal, K., and Schneider, J.P. (2004). Self-assembling peptides and proteins for nanotechnological applications. Curr. Opin. Struct. Biol. 14, 480–486. https://doi.org/10.1016/j.sbi.2004.06.006.

Roosen-Runge, F., Hennig, M., Zhang, F., Jacobs, R.M.J., Sztucki, M., Schober, H., Seydel, T., and Schreiber, F. (2011). Protein self-diffusion in crowded solutions. Proc. Natl. Acad. Sci. U S A 108, 11815–11820. https://doi.org/10.1073/pnas.1107287108.

Sarroukh, R., Goormaghtigh, E., Ruysschaert, J.M., and Raussens, V. (2013). ATR-FTIR: a "rejuvenated" tool to investigate amyloid proteins. Biochim. Biophys. Acta 1828, 2328–2338. https://doi.org/10.1016/j.bbamem.2013.04.012.

Sassi, P., Giugliarelli, A., Paolantoni, M., Morresi, A., and Onori, G. (2011). Unfolding and aggregation of lysozyme: a thermodynamic and kinetic study by FTIR spectroscopy. Biophys. Chem. 158, 46–53. https://doi.org/10.1016/j.bpc.2011.05.002.

Sassi, P., Onori, G., Giugliarelli, A., Paolantoni, M., Cinelli, S., and Morresi, A. (2011). Conformational changes in the unfolding process of lysozyme in water and ethanol/water solutions. J. Mol. Liquids 159, 112–116. https://doi.org/10.1016/j.molliq.2010.12.008.

Sciortino, F., Mossa, S., Zaccarelli, E., and Tartaglia, P. (2004). Equilibrium cluster phases and low-density arrested disordered states: the role of short-range attraction and long-range repulsion. Phys. Rev. Lett. 93, 055701. https://doi.org/10.1103/PhysRevLett.93.055701.

Shukla, A., Mylonas, E., Di Cola, E., Finet, S., Timmins, P., Narayanan, T., and Svergun, D.I. (2008). Absence of equilibrium cluster phase in concentrated lysozyme solutions. Proc. Natl. Acad. Sci. U S A 105, 5075–5080. https://doi.org/10.1073/pnas.0711928105.

Stradner, A., Sedgwick, H., Cardinaux, F., Poon, W.C.K., Egelhaaf, S.U., and Schurtenberger, P. (2004). Equilibrium cluster formation in concentrated protein solutions and colloids. Nature 432, 492–495. https://doi.org/10.1038/nature03109.

Taschin, A., Bartolini, P., Eramo, R., and Torre, R. (2006). Supercooled water relaxation dynamics probed with heterodyne transient grating experiments. Phys. Rev. E 74, 031502. https://doi.org/10.1103/PhysRevE.74.031502.

Wei, G., Su, Z., Reynolds, N.P., Arosio, P., Hamley, I.W., Gazit, E., and Mezzenga, R. (2017). Self-assembling peptide and protein amyloids: from structure to tailored function in nanotechnology. Chem. Soc. Rev. 46, 4661–4708. https://doi.org/10.1039/c6cs00542j.

Zandomeneghi, G., Krebs, M.R., McCammon, M.G., and Fändrich, M. (2009). FTIR reveals structural differences between native β-sheet proteins and amyloid fibrils. Protein Sci. 13, 3314–3321. https://doi.org/10.1110/ps.041024904.

Zou, Y., Li, Y., Hao, W., Hu, X., and Ma, G. (2013). Parallel β-sheet fibril and antiparallel β-sheet oligomer: new insights into amyloid formation of hen egg white lysozyme under heat and acidic condition from FTIR spectroscopy. J. Phys. Chem. B 117, 4003–4013. https://doi.org/10.1021/jp4003559.

STAR★METHODS

KEY RESOURCES TABLE

REAGENT or RESOURCE	SOURCE	IDENTIFIER
Chemicals, peptides, and recombinant proteins		
Hen Egg-White Lysozyme	Sigma Aldrich	L6876
Deuterium Oxide (99.9 atom % D)	Sigma Aldrich	7789-20-0
Deposited data		
All data reported in this paper will be shared by the lead contact upon request.		
Software and algorithms		
Opus 5.5 software	Bruker Optics	https://www.bruker.com/en/products-and-solutions/infrared-and-raman/opus-spectroscopy-software.html
Saxsgui program	Rigaku	N/A
Matlab software	MathWorks	https://it.mathworks.com/products/get-matlab.html?s_tid=gn_getml
Origin 2018 software	OriginLab	https://www.originlab.com/
Other		
FTIR spectrometer	Bruker	N/A
SAXS spectrometer	Bruker AXS Micro instrument	N/A
CD spectrometer	JASCO	N/A
HD-TG set-up	home made at LENS	N/A
FTIR spectrometer	Bruker	N/A

RESOURCE AVAILABILITY

Lead contact

Further information and requests for resources and reagents should be directed to and will be fulfilled by the Lead Contact, Sara Catalini (catalini@lens.unifi.it).

Materials availability

This study did not generate new unique reagents.

Data and code availability

All data reported in this paper will be shared by the lead contact upon request. This paper does not report original code. Any additional information required to reanalyze the data reported in this paper is available from the lead contact upon request.

EXPERIMENTAL MODEL AND SUBJECT DETAILS

This work does not use experimental models typical in the life sciences.

METHOD DETAILS

Samples preparation

The lyophilized powder of Hen Egg-White Lysozyme (Sigma Aldrich, L6876) is dissolved in deuterium oxide (99.9 atom % D, Sigma Aldrich), to prepare solutions with different protein concentration ranging from 5 to 307 mg/mL. The protein solubilisation has been incentivized leaving the sample at 40°C for an hour. After the total dissolution, the solution pH is adjusted with deuterium chloride (2M), to reach a final pH value of 1.8. The protein-based hydrogels have been prepared starting from the 240 mg/mL concentrated solution, leaving the system at high temperatures (45, 50 and 55°C) for two hours and then quickly cooled to room temperature. After few hours transparent gels are formed.

FTIR spectra

Infrared absorption measurements are collected using a FTIR Bruker spectrometer model Tensor27, equipped with a DTGS detector. Transmission spectra are obtained employing a homemade cell equipped with CaF_2 windows that is placed into a jacket whose temperature is controlled by a Haake F6 circulating water thermostat. The spectra are acquired with a resolution of 2 cm^{-1} by averaging over 20 scans for each spectrum. The software Opus 5.5 Bruker Optics is used for the acquisition and manipulation of the spectra. The spectra are corrected employing the atmospheric compensation routine (Opus 5.5) to reduce the interference due to CO_2 and water vapor.

The fraction f(T) of unfolded LYS monomers as a function of temperature (Figure 1D) has been estimated, based on a two-state model, from the T-dependence of the Amide I (AmI) band absorbance at 1650 cm^{-1} considering the relationship: $f(T)=(A_F-A_T)/(A_F-A_U)$. Here A_F is the absorbance at 25°C, taken as reference value for the folded state, A_U the absorbance at 87°C, taken as reference value for the unfolded state, and A_T the value at the intermediate T (Sassi et al., 2011).

The percentage of cross-β structures has been estimated by the ratio of the areas of the peaks associated with the intermolecular β-sheet components over the entire amide I band. The amide I bands of LYS_{120} and LYS_{240} samples have been normalized for the maximum absorbance value as reported in Figure S4. This comparison indicates that the amide I bands only differ because of the spectral components related to the amyloid oligomers. In these conditions the amyloid components at 1620 cm^{-1} and 1685 cm^{-1} can been isolated by subtracting form the spectrum of LYS_{240} the normalized spectrum of the LYS_{120} at the corresponding temperature. The percentage of cross-β structures has then been estimated by the ratio of the areas of the residual intensity, due to the intermolecular β-sheet components, over the entire Amide I band obtained for the LYS_{240} solution.

SAXS experiment

SAXS measurements are performed on a Bruker AXS Micro instrument. The source is a micro focused X-ray operating at voltage and filament current of 50 kV and 1000 mA, respectively. The CuKα radiation (λ CuKα = 1.5418 Å) is collimated by a 2D Kratky-collimator, and the data are collected by a 2D Pilatus 100 K detector. The scattering vector is calculated as $q = (4\pi/\lambda) \sin\theta$, 2θ is the scattering angle calibrated using silver behenate. Data are collected and azimuthally averaged using the Saxsgui software to yield one-dimensional intensity versus scattering vector q, with a q range from 0.004 to 0.5 $Å^{-1}$. All the samples are filled into 2 mm diameter quartz capillaries which are sealed with epoxy glue (UHU). Measurements are performed as a function of temperature and the scattered intensity is collected between 2 or 6 h, depending on the sample concentration.

The small angle scattering intensity, I(q), is generated by two contributions. The first contribution is the so-called form factor, P(q), that gives intra-monomer information (like shape and size). The second contribution is due to the structure factor, S(q), that is generated by the inter-monomer interactions. Once that the scattering intensity of the sample is recorded and corrected for the solvent contribution, the equation that describes I(q) can be summarize as I(q)= n P(q) S(q) (Kikhney and Svergun, 2015). In this relationship n is a constant which accounts for the monomer contrast. Figure S1A shows that I(q) forms a plateau from 0 until 0.07 $Å^{-1}$ for the 5 mg/mL LYS solution. Such a plateau is characteristic of monodisperse dilute protein solutions. Figure S1B shows the Guinier plot of the experimental scattering curves. In the 0.01–0.05 $Å^{-2}$ range the data of the 5 mg/mL LYS solution fall into a straight line, highlighting the monodisperse character of the sample and suggesting the possibility of neglecting inter-monomer correlations (Kikhney and Svergun, 2015). In such a context the structure factor can be approximated to 1, simplifying the relation to I(q) = n P(q) (Kikhney and Svergun, 2015). Increasing the protein concentration from 30 up to 307 mg/mL the SAXS curve is generated by both P(q) and S(q) contributions. The descent of I(q) at small q-values indicates a repulsive interaction potential between the monomers. Indeed, at pH 1.8 the LYS monomers surface has a high positive charge and consequently the strong repulsive potential between monomers leads to I(q) suppression at low scattering wave vectors (Bonnete et al., 1999; Finet et al., 2004). At high concentrations, a broad hump (0.1–0.2 $Å^{-1}$) that characterizes the SAXS profiles is related to the inter-monomers correlation distance due to their interactions and S(q) ≠ 1 (Kikhney and Svergun, 2015).

HD-TG experiment

A single 1064 nm laser beam is divided in two pulses, which interfere and produce into the sample an impulsive spatial modulation of the material optical properties, characterized by the wave vector q. The temporal

evolution of the induced modulation is probed through a third laser beam at 532 nm. The angle between the exciting beams and consequently the q-vector induced in the sample, are changed using different spacing of the grooves of the phase mask. A q-vector value of 2.1 and 1.4 μm^{-1} are investigated. The grating diffracts the beams, passes through a doublet of achromatic lenses, and the second lens of the achromatic doublet recombined and focused the beams on the sample, reproducing the same spatial modulation of the phase mask. A reference beam is used to produce the heterodyne detection. The HD-TG signal is optically filtered and measured by a photodiode with a bandwidth of 1 GHz. The signal is then amplified and recorded by a digital oscilloscope with a 7 GHz bandwidth. We record the data using a fast time window (0-80 ns range with a 50 ps time step of sampling) and a long one (0-2 μs range with 800 ps time step). The measurements are merged in a single data file. Each signal are the average of 1000 records, producing an excellent signal to noise ratio. The samples are kept directly in the cuvette, introduced in a copper cell holder, connected to a thermostat and a thermocouple to feedback the temperature control. The temperature is varied from 20 to 80°C.

The parameter that we discuss in the manuscript is the viscosity coefficient, D_v, that is extracted from the oscillating part of the HD-TG signal and is calculated as $D_v = 1/(\tau_s \cdot q^2)$ (valid in the approximation of $C_p/C_v \sim 1$ (Taschin et al., 2006), where C_p/C_v is the specific heat ratio). The parameters are τ_s that is the damping time of the acoustic wave oscillation and q that is the scattering vector imposed by the experimental geometry. The uncertainty associated with D_v is 1% that is related to the fitting procedure. From the viscosity coefficient, it is possible to obtain information on the viscoelastic behaviour of the medium. Usually, the phase transitions of materials are monitored through calorimetry, which is sensitive to heat induced structural changes, and/or by mechanical rheology, which is sensitive to the low-frequency viscoelastic properties of the system. HD-TG spectroscopy provides an alternative and complementary non-invasive and non-destructive approach to study the phase transitions of soft materials (Catalini et al., 2019).

ADDITIONAL RESOURCES

This work does not include any additional resources.